(article starts on next page)

Hydrogen permeability of thin-ply composites after mechanical loading

Ioannis Katsivalis [a,*], Virginia Signorini [b], Fredrik Ohlsson [c], Christoph Langhammer [d], Matteo Minelli [b], Leif E. Asp [a]

[a] *Department of Industrial and Materials Science, Chalmers University of Technology, Sweden*
[b] *Department of Civil, Chemical, Environmental, and Materials Engineering (DICAM), Alma Mater Studiorum - University of Bologna, Italy*
[c] *Oxeon AB, Sweden*
[d] *Department of Physics, Chalmers University of Technology, Sweden*

ARTICLE INFO

ABSTRACT

Hydrogen is a sustainable alternative to conventional fuels, and it may be obtained with near zero carbon footprint. However, hydrogen storage remains a key challenge, and the use of composite tanks has gained significant interest over the last few years. In addition, thin-ply composites promote fibre damage by delaying matrix microcracking and free edge delamination. In this work, the H2 permeation/diffusion performance of virgin and mechanically loaded thin cross-ply laminates is studied. In addition, Scanning Electron Microscopy (SEM) is used to identify defects and micro-damage in the laminates and explain the experimental values. The study shows that the hydrogen (H2) barrier performances of thin-ply composites are lower than conventional metallic systems. Obtained permeability values, however, resulted well below the allowable limits for most combinations of temperature and pressure and remain unaffected despite the application of high tensile strains showing that permeation is not accelerated.

1. Introduction

According to the International Energy Agency (IEA) transportation is responsible for 24% of worldwide energy related emissions [1]. Therefore, there is a growing need to reduce these emissions in order to be able to achieve the commitments of the Paris agreement [2]. In recent years, hydrogen technology has emerged as a viable solution to significantly reduce CO_2 emissions by using hydrogen (H_2) as a "cleaner" transportation energy source. Hydrogen technologies can be used for aviation, maritime and road transportation.

The storage of hydrogen, however, remains a key challenge in adopting this new technology to commercial vehicles. Hydrogen can be stored in two forms, gaseous or liquid. The former has very low density which indicates that high pressure tanks would need to be used, while for the latter, cryo temperatures would need to be achieved as hydrogen liquefies at $-253\,°C$ [3]. In addition, liquid hydrogen has about 4 times lower volumetric energy density compared to other conventional fuel types and therefore the required storage tank size would be four times larger for a similar range.

Hydrogen also has a high diffusivity in air and, thus, leakage and diffusion through the storage tanks need to be supressed [4].

Traditionally, metals have been used for storage tanks, but their high density increases the overall weight of the structure. In addition, metals are susceptible to hydrogen embrittlement and hydrogen assisted cracking [5], which may lead to catastrophic failures of the tanks.

Carbon Fibre Reinforced Plastic (CFRP) composite materials have very high specific strength (strength to density ratio) and thus can lead to significant weight reductions of the tank even when used with a metal liner. For instance, storage tanks of type III (metallic liner fully wrapped with CFRP) can offer weight reductions of 25%-75% compared to type I (fully metallic) and type II (metallic liner hoop partly wrapped with CFRP) tanks [6]. In addition, liner-less tank solutions reduce the weight of the structure even further. Reductions of about 20% have been reported in the literature for the storage tanks of type V (liner-less composite) compared to type IV (composite with polymer liner) [7].

The use of composite materials for storage tanks also entails certain limitations. Hydrogen molecules can diffuse through the bulk of the composite materials, especially in the presence of micro-cracks and imperfections. The composites are also expected to experience high thermal fatigue cycles at a very wide range of temperatures, which in cases can exceed $300\,°C$ [3]. In addition, the use of metal or plastic liners, typically employed by the industry for hydrogen storage tanks,

can generate significant thermal stresses in the composite structure due to the differences in the thermal expansion coefficients.

Gas permeability in carbon fibre composites has been assessed in numerous studies in the past [8–11], revealing their potential as suitable option for hydrogen storage. However, cryogenic cycling was shown to increase their permeability highlighting the effect of defects on the composite performance [12]. Saha et al. [13] studied the effect of cryogenic exposure to three dimensional stitched composites, and a sharp increase in permeability was observed after the first cryogenic cycle for plies of standard thickness. The authors also noticed that adding thin plies in the material preserves its H₂ barrier properties as only minimal changes in the permeability are observed at increasing cryogenic cycles.

Grogan et al. [14] have also shown that the thickness of the laminates has a significant effect on the damage initiation and propagation during cyclic loading. Thin-ply composites are well known to provide higher strength values compared to conventional thick-ply composites [15]. In addition, thin-ply composites fail at higher strains, delay matrix microcracking and free-edge delamination [16], ultimately leading to improved fatigue performance [17]. However, the cost of thin-ply composites is relatively high, and there is a lack of design standards and certification requirements and therefore, the industry is reluctant to adopting these solutions.

The measurement of hydrogen permeation through thin-ply composites is a challenging problem. In addition, the quantification of the effect of mechanical loading on the permeation mechanism could allow an insight on micro-crack generation that could not be identified otherwise. Hamori et al. [18] used thin plies as barriers on the composite architecture and investigated the effect of cryogenic and biaxial mechanical loading on the gas permeability. Their work showed that the thin ply barriers improve the tolerance against both damage and leakage. Condé-Wolter et al. [19] performed permeation testing for thermoplastic matrix materials and composites, revealing that the permeation rates for the composites can be sufficiently low assuming no damage in the composite microstructure. As a result, showing that the hydrogen diffusion is not accelerated despite mechanical loading (and thus no micro-crack permeation paths are developed) could provide additional confidence in the use of thin-ply composites for hydrogen storage tanks.

This study analyses the hydrogen permeation/diffusion performance of thin-ply composites before and after mechanical loading. Thin cylindrical specimens were cut out from cross-ply [0/90/0/90/0] plates for permeation measurements. In addition, tensile specimens were cut from the same plates which were subjected to a constant strain level under quasi-static loading. The loading was released, and the tensile specimens were repurposed as permeation specimens. Therefore, the hydrogen permeability and diffusivity in the cross-ply laminates was measured before and after mechanical deformation. It is demonstrated that the diffusivity of the thin-ply composites is higher compared to those achieved by metals but also it was shown that the mechanism is not accelerated despite the application of significant loading. Finally, the leak rate stays well below the allowable limits for most temperature and pressure combinations.

2. Hydrogen transport mechanism

The permeation mechanism in a hydrogen storage tank takes place through the bulk of the CFRP vessel walls and consists of adsorption, absorption, diffusion, and desorption [20]. Adsorption is the process by which hydrogen molecules adhere to the internal surfaces of the CFRP walls without being absorbed into the material. Absorption, on the other hand, is the process by which hydrogen molecules are absorbed into the material, forming a homogeneous solution with the matrix. Diffusion is the movement of hydrogen molecules from areas of higher concentration to areas of lower concentration within the material. The diffusivity depends on the material properties and temperature. Finally, desorption

is the reverse of absorption, and it refers to the release of hydrogen molecules from the material back into the gas phase.

The whole process is diffusion controlled as the hydrogen sorption and desorption processes are much faster compared to diffusion in the matrix material [20]. The diffusion process is governed by Fick's law as shown in equation (1), which correlates the flux J (expressed in $mol\ m^{-2}\ s^{-1}$ in this paper) with the diffusivity D (expressed in $m^2\ s^{-1}$) and the concentration gradient over the thickness (driving force of the process) $\frac{dC}{dx}$. Finally, for a solution-diffusion transport model, the hydrogen permeability P (in this paper expressed in Barrer) is obtained as the product of the diffusivity D and the solubility coefficient S (expressed in $mol\ m^{-3}\ Pa^{-1}$ for plastics), as follows in equation (2):

$$J = -D\frac{dC}{dx} \tag{1}$$

$$P = DS \tag{2}$$

Fig. 1 schematically describes the hydrogen permeation phenomenon through the CFRP laminates. It is worth noting that manufacturing defects or damage accumulation such as porosity and microcracking can accelerate the permeation phenomenon as they can provide a fast diffusion path through the thickness of the CFRP walls. It can be assumed that undamaged composites display Fickian behaviour while the effect of temperature can be described by an Arrhenius equation assuming no phase change occurs [12]. Pressure is also known to have minor effect on the permeability/diffusivity of light gases (such as He or H₂) in polymers [21].

3. Methodology

3.1. Materials

Cross-ply CFRP plates [0/90/0/90/0] were manufactured using two different materials and manufacturing methods. The plates manufactured with material A were prepreg with a thickness per ply of 41 μm, while material B was manufactured using a wet laying resin application and the thickness of each ply was slightly higher (50 μm). For material A, the Tenax® IMS 65 E23 830 24 k fibre was used with fibre modulus of 290 MPa and fibre strength of 6000 MPa while for material B, the PYROFIL TR50S 15 K fibre was used with fibre modulus of 240 MPa and fibre strength of 4900 MPa. Material A was cured at 150 °C for one hour while material B was cured at lower temperatures for about 20 h (66 °C for 16 h and 93 °C for 4 h). Table 1 provides an overview of the material tested for this work. The thickness of the material A laminates was consistent at 0.25 mm while the material B laminates had slightly higher thickness variation due to the manufacturing method. A minimum of two batches per material were tested to ensure repeatability. Water-jet cutting was used to obtain the specimens for the testing reported in sections 3.2 and 3.3. Fig. 2 provides a sketch of the plates manufactured indicating the positioning of the specimens used for the tensile and permeation testing.

3.2. Permeation measurements

Hydrogen permeation measurements were conducted in a manometric system with a closed volume and variable pressure method, following ASTM D1434-82 [22]. Fig. 3 provides a sketch of the test rig layout. Cylindrical specimens were used for the permeation measurements with a diameter of 25 mm.

The permeation set-up consists of a sample holder, where the specimen is placed, which is then connected to the upstream reservoir and to a calibrated downstream volume, where the permeated gas is collected. The system is placed into a thermostatic incubator to ensure temperature control. Before testing, the system was evacuated over night to remove any residual gas absorbed. The upstream pressure is monitored
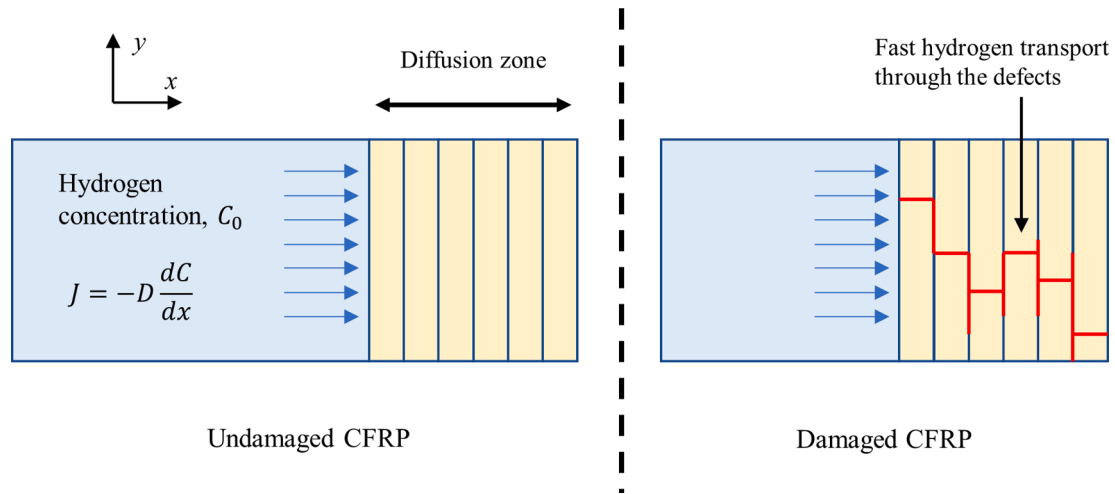
Fig. 1. Diffusion mechanism in damaged and undamaged CFRP. (For interpretation of the references to colour in this figure legend, the reader is referred to the web version of this article.)

Table 1
Overview of tested materials.

Material	Ply thickness	Lay-up	Manufacturing
A1, A2, A3	41 µm	[0/90/0/90/0]	Prepreg (reactive binder applied during spreading/150 °C for 1 h at 4 bar pressure
B1, B2	50 µm	[0/90/0/90/0]	Wet laying resin/66 °C for 16 h and 93 °C for 4 h at 4 bar pressure

by a Druck gauge manometer and maintained constant at about 1.5 bar during the whole test, while the downstream side is kept under vacuum to guarantee the pressure gradient, that acts as the driving force of the process. The permeability is evaluated by monitoring the downstream pressure increase over time, using a 10 Torr MKS Instruments manometer. Hence, at the steady state conditions, the permeability P only depends on the flow of the permeating gas across the membrane as shown in equation (3):

$$P = \frac{V_d l}{RTA\Delta p}\frac{dP_d}{dt} \tag{3}$$

where V_d is the downstream volume (measured in m^3), l is the sample thickness (measured in m), R is the universal gas constant (SI units: $J\ K^{-1}\ mol^{-1}$), T is the absolute temperature (in K), A is the sample area (in m^2), Δp is the pressure gradient (in $Pa\ m^{-1}$) between the feed and the permeate side and $\frac{dP_d}{dt}$ indicates the increasing rate of the downstream pressure over time.

Permeability is reported in the non SI unit Barrer, $1 barrer = 10^{-10}\frac{cm^3(STP)\ cm}{cm^2\ s\ cmHg} = 3.35\times 10^{-16}\frac{mol\ m}{m^2\ s\ Pa}$. The diffusivity can also be determined from the permeation rate experiments by applying the time lag method. The time lag, τ_L, represents the intercept on the time axis of the asymptotic linear behaviour of downstream pressure over time [23].

Plan for material A and B plates [0/90/0/90/0]

Detail of the specimen for mechanical loading and position of the specimens for the permeability measurements
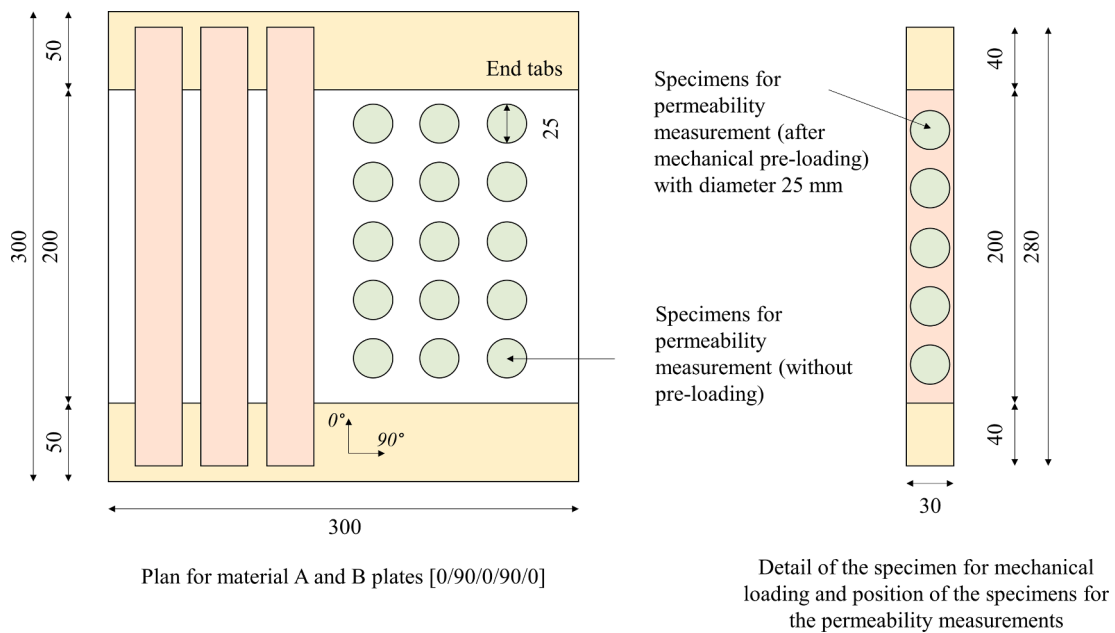
Fig. 2. Plate design and details of the two types of tested specimens. Circular cross-section samples were prepared for permeation tests, whereas the rectangular ones were made for mechanical tests. All dimensions in mm. (For interpretation of the references to colour in this figure legend, the reader is referred to the web version of this article.)
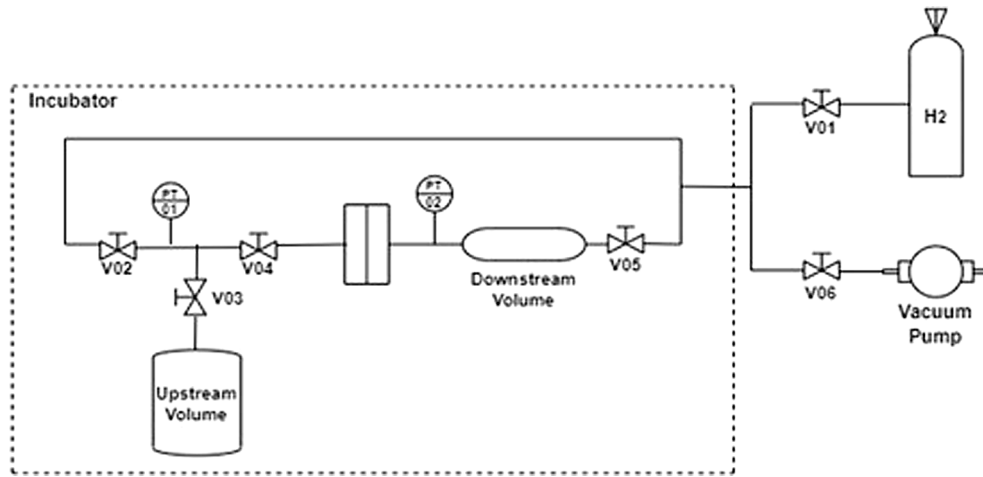
Fig. 3. Test rig for the hydrogen permeation measurements.

The value of the diffusivity can be extracted as shown in equation (4):

$$D = \frac{l^2}{6\tau_L} \tag{4}$$

where l is the thickness of the specimen tested and τ_L is the time-lag value. Each test is repeated at least once to ensure the repeatability of the measurements. In cases, where there was large scatter between the first and second measurements (coefficient of variation above 10% for permeability and 20% for diffusivity), a third measurement was added.

3.3. Tensile testing

The mechanical pre-loading of the specimens used for permeation measurements was achieved utilising a tensile test. During testing, the load/displacement curve was recorded along with the strain at the centre of each specimen. The size of the specimens tested was 300 × 30 mm. To ensure proper gripping, GFRP end tabs were bonded to the specimens. A universal servo-electric loading machine was used, and the loading rate was adjusted to 1 mm/min while the strain was monitored with an extensometer. The specimens were chosen to be 30 mm in width so that after the pre-loading, permeation specimens (cylinders with 25 mm diameter) can be cut as shown in Fig. 2.

3.4. SEM analysis

Scanning Electron Microscopy (SEM) was used to evaluate the interfaces of the tested specimens. The interfaces could reveal porosity, dry spots and pin holes which could affect the permeation measurements and material performances. The specimens were mounted on stubs and a thin layer of about 5 μm of gold sputter was applied before the inspection with a JEOL 7800F Prime. The microscope magnifications used were in between x100 and x8000 with an acceleration voltage of 5 kV.

4. Results

4.1. Permeation measurements

Fig. 4 shows the permeation measurements for the different batches and materials tested over a range of temperatures. The temperatures tested were between 5 °C and 45 °C, but these can be extrapolated to lower values considering that the permeability is expected to follow an Arrhenius behaviour [24], assuming no phase changes of the composite, as shown in equation (5):

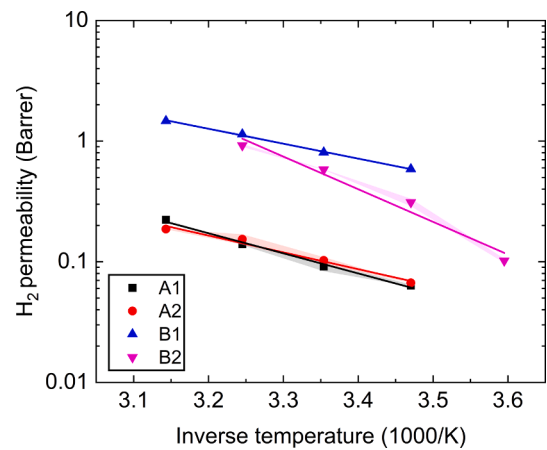$$P = P_0 \exp\left(-\frac{E_P}{RT}\right) \tag{5}$$

Fig. 4. Hydrogen permeability through the thickness of the cross-ply laminate as a function of temperature. The shaded parts of the plot represent the experimental scatter of the measurements. (For interpretation of the references to colour in this figure legend, the reader is referred to the web version of this article.)

In equation (5), P is the permeability, P_0 is the pre-exponential factor that provided the permeability when temperature goes to infinity, E_P is the activation energy for permeation, R is the universal gas constant and T is the temperature. The activation energy for permeation can be determined from the slopes in Fig. 4. The measurements between materials A and B display a difference of about one order of magnitude while the permeability results between the different batches of the same materials have smaller differences. The shaded parts in Fig. 4 show the experimental scatter of the measurements which are based on the standard deviation recorded for each test.

Similarly, Fig. 5 shows the diffusivity for the different batches and materials examined over the same range of temperatures. Once again, this parameter can be extrapolated at lower temperatures assuming an Arrhenius behaviour [24] and no phase changes as shown in equation (6):

$$D = D_0 \exp\left(-\frac{E_D}{RT}\right) \tag{6}$$

In equation (6), D is the diffusivity, D_0 is the pre-exponential factor that states the diffusivity when the temperature goes to infinity, E_D is the activation energy for diffusion, R is the universal gas constant and T is the temperature. In a similar fashion to the activation energy for
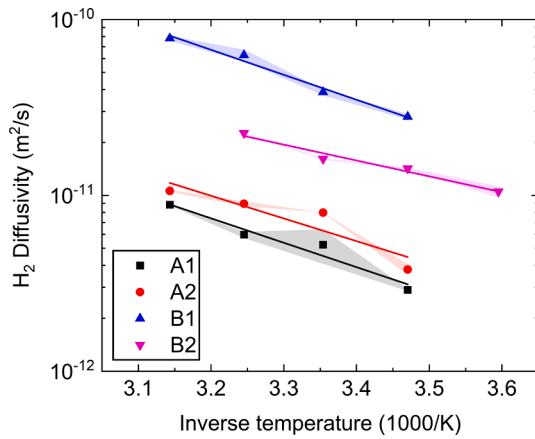
Fig. 5. Hydrogen diffusivity through the thickness of the cross-ply laminate as a function of temperature. The shaded parts of the plot represent the experimental scatter of the measurements. (For interpretation of the references to colour in this figure legend, the reader is referred to the web version of this article.)

permeation, the activation energy for diffusion can be calculated from the slopes in Fig. 5. The shaded parts in Fig. 5 show the experimental scatter of the measurements which are based on the standard deviation recorded for each test.

As already observed for permeability, the diffusivity in materials A and B also differs by one order of magnitude, while no significant discrepancy is observed in various specimens of the same materials (A1-A2 and B1-B2). It is worth noting that comparing the permeability values obtained for the CFRP laminates with more traditional materials used for hydrogen storage is not straightforward as permeability has different units for metals and polymers. This is due to the fact that hydrogen does not dissociate prior to the dissolution in the material [21], thus assuming a different behaviour of its solubility coefficient. Therefore, the hydrogen concentration in polymers is linear with the pressure while in metals it is linear with the square root of pressure.

Hence, a comparison between the performance of the CFRP laminates and stainless steel/aluminium, materials that would be typically used for such applications, was based on the values of diffusivity, which maintain the same units. Table 2 reports characteristic diffusivity values for stainless steel, aluminium and other CFRP materials obtained from the literature. The values reported in this study for diffusivity are of the same order of magnitude as other CFRP materials and about two orders of magnitude higher compared to typical stainless steels. Aluminium presented a higher range of diffusivity values which extend above and below the measurements of this study.

4.2. Effect of pre-loading

Material B2 was chosen for further analysis to inspect the effect of

mechanical preloading on H_2 transport properties. The specimens were pre-loaded at two different strain levels and afterwards the permeation testing was repeated. Fig. 6 shows the stress/strain curves for the two specimens which were mechanically pre-loaded with a tensile test. The first specimen was loaded up to a strain of 1%, while the second specimen was loaded up to a strain of 1.4%. It was also attempted to achieve higher strains, but the specimens failed catastrophically at around 1.5% of strain. However, it is worth noting that current allowable strain limits for contemporary aircraft composite structures do not exceed 0.5% and thus the attained strain levels were considered as adequate for the targeted application, as they provide a safety factor of 3. The specimen response was linear throughout the loading and the stiffness of the specimens was in the region of 70 GPa.

Fig. 7 shows the permeation (7a) and diffusion coefficients (7b) as a function of the inverse of temperature for the virgin unloaded specimen, and the two mechanically pre-loaded specimens from batch B2. The shaded parts in Fig. 7 show the experimental scatter of the measurements.

Fig. 7 shows that there is no significant effect of the mechanical preloading on the diffusion/permeation measurements for material B2. The shaded parts in Fig. 7 show the experimental scatter of the measurements which are based on the standard deviation recorded for each test. Small differences were recorded in the slope for the permeability measurements. For the diffusion measurements, the slopes are almost identical, but a small decrease in the diffusivity is recorded for the specimen with the highest level of strain. This is a clear demonstration that, despite the significant levels of strain attained, the thin plies were able to supress the generation of transverse matrix cracks and delay delamination. Therefore, the lack of damage and micro-cracks explain that no acceleration of gas transport was observed.

The in-situ strength theory developed by Camanho et al. [15] was utilised to critically assess these findings and evaluate the relationship between transverse strain to failure and ply thickness for material B2. Strain expressions for the transverse strength were derived as shown in Katsivalis et al. [31] to make the comparison more relevant to the experimental measurements of this work. Therefore, Fig. 8 plots the transverse strain to failure as a function of the ply thickness and shows that plies thinner than 100 μm (for material B2 the ply thickness is 50 μm) will not develop transverse cracks at strains below 1.4%, thereby validating our experimental observations.

It is also worth noting that local damage limited to the 90° plies (without damage in 0° plies) would still lead to hydrogen transport acceleration as the effective thickness of the specimen would be reduced by 40%. Therefore, the time required for the hydrogen to diffuse through the thickness of the specimen would be greatly accelerated leading to lower values of diffusivity.
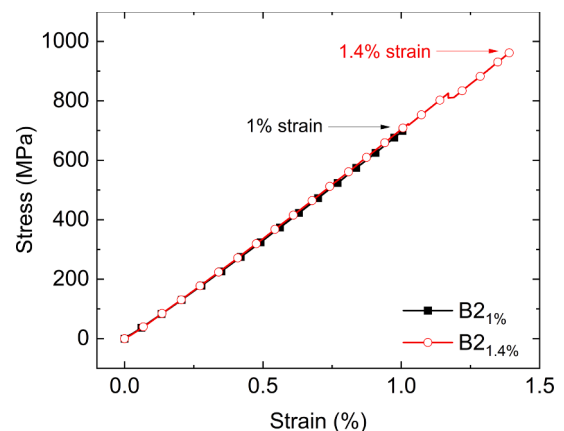
Table 2
Comparison of diffusivities at room temperature for CFRP, stainless steel and aluminium materials.

Source	Material	Diffusivity ($m^2 s^{-1}$)
Current study (A1)	CFRP [0/90/0/90/0]	5.2×10^{-12}
Current study (B2)	CFRP [0/90/0/90/0]	1.6×10^{-11}
Flanagan et al. [12]	CFRP [45/135/0₄/135/45]	1.2×10^{-11}
Condé-Wolter et al. [19]	CFRP [UD]	2.9×10^{-13}
Chen et al. [25]	2205 Duplex Stainless Steel	2.2×10^{-14}
Hutchings et al. [26]	B50 Duplex Stainless Steel	1.5×10^{-14}
Luu et al. [27]	2205 Duplex Stainless Steel	6.4×10^{-14}
Young and Scully [28]	Aluminium	2.3×10^{-11}
Saitoh et al. [29]	Aluminium	1.0×10^{-14}
Outlaw et al. [30]	Aluminium	3.2×10^{-14}

Fig. 6. Stress–strain curves for the mechanical pre-loading performed on the permeation specimens. (For interpretation of the references to colour in this figure legend, the reader is referred to the web version of this article.)
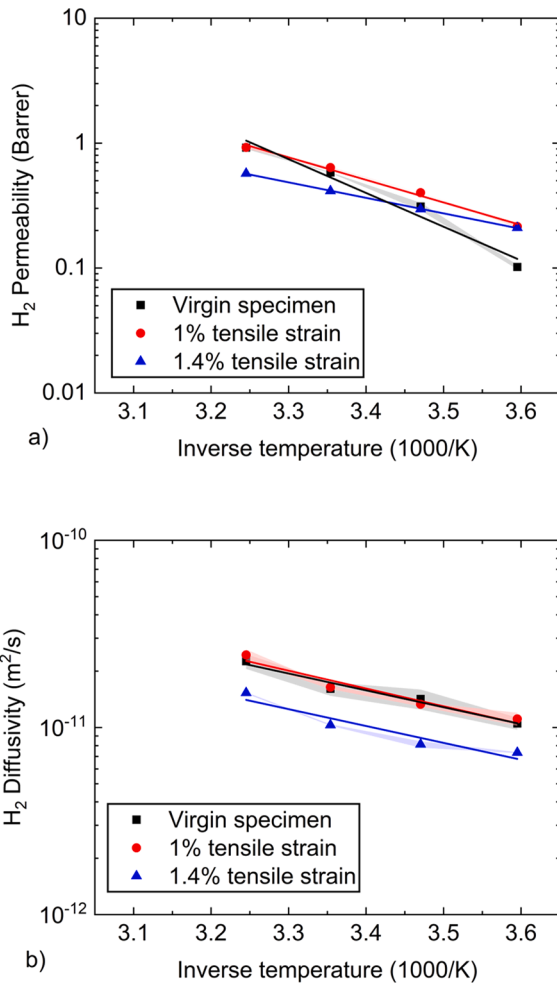
Fig. 7. Effect of mechanical pre-loading on the a) permeability and b) diffusivity of the B2 cross-ply laminate as a function of temperature. The shaded parts of the plot represent the experimental scatter of the measurements. (For interpretation of the references to colour in this figure legend, the reader is referred to the web version of this article.)
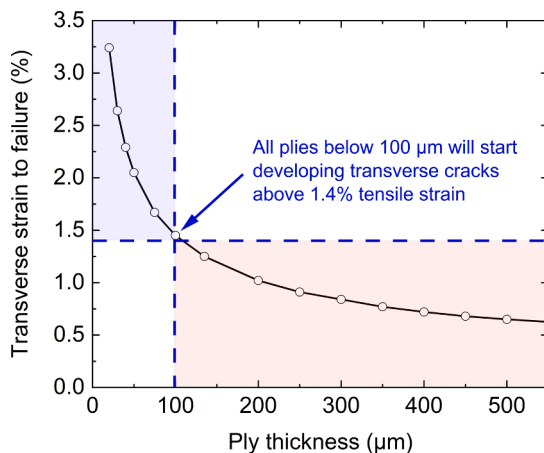

Fig. 8. Transverse strain-to-failure as a function of ply thickness based on the material properties of material B2. (For interpretation of the references to colour in this figure legend, the reader is referred to the web version of this article.)

Table 3 summarises the permeation and diffusion results for all materials and batches tested and provides the values for the permeation and diffusion activation energies. It is worth noting that for comparison purposes all values of permeability and diffusivity are reported at 25 °C.

It was not possible to measure the permeability and diffusivity of batch A3 due to very large fluxes detected during permeation testing, much larger than the experimental limits, thus indicating defects and cracks in the specimens. Various specimens from several parts of the plate were cut and tested multiple times to avoid possible local damage, but such problems persisted, indicating that either during manufacturing, cutting or transportation the plate was damaged irreversibly. Therefore, a dedicated analysis utilising SEM was performed to inspect such effects, as presented in the following section.

4.3. SEM analysis

SEM imaging was used to identify features in the matrix, the fibres or the interfaces that could explain the results and especially the inability to measure permeation and diffusion in laminate A3. The SEM analysis was conducted at a larger scale initially to detect pinholes, dry spots and other larger features which could be responsible for the measurements of laminate A3. Fig. 9a displays a part of laminate A3 at a magnification of x100 where pinholes can be observed. Larger magnifications (x2000), as shown in Fig. 9b, gave a greater insight in these imperfections. The fibres of the subsequent plies can be observed through the pinholes indicating that these defects extend through the thickness and thus providing fast diffusion paths and explaining the inability to perform the permeation measurements. In addition, even larger magnifications (x8000) were used (as shown in Fig. 9c), which allowed to identify nanoporosity in the resin which could also contribute to the acceleration of the permeation mechanism.

Further SEM analysis was conducted on the tested specimens from batch A1 as shown in Fig. 10 and did not reveal any damage at the lower magnification levels (x 100 and ×2000). At the highest magnification levels (x8000), however, nano-porosity was observed. This was expected since the same resin and fibres were used for batches A1 and A3. However, the permeation measurements conducted in plate A1 were completed successfully and thus the nano-porosity was not considered as a critical factor accelerating the permeation mechanism.

Finally, SEM analysis was also conducted at the same magnification levels for specimens from material B which are shown in Fig. 11 for comparison purposes. No defects or porosity were identified at larger or smaller scales. It is worth noting that despite material B showing the least number of defects at the scales observed by SEM, it was still outperformed in terms of diffusivity/permeability values compared to batches A1 and A2. It is however important to remind that the diffusion process occurs at the molecular level, and it is related to the polymer

Table 3
Summary of the permeation and diffusion measurements for all materials and batches tested at 25 °C.

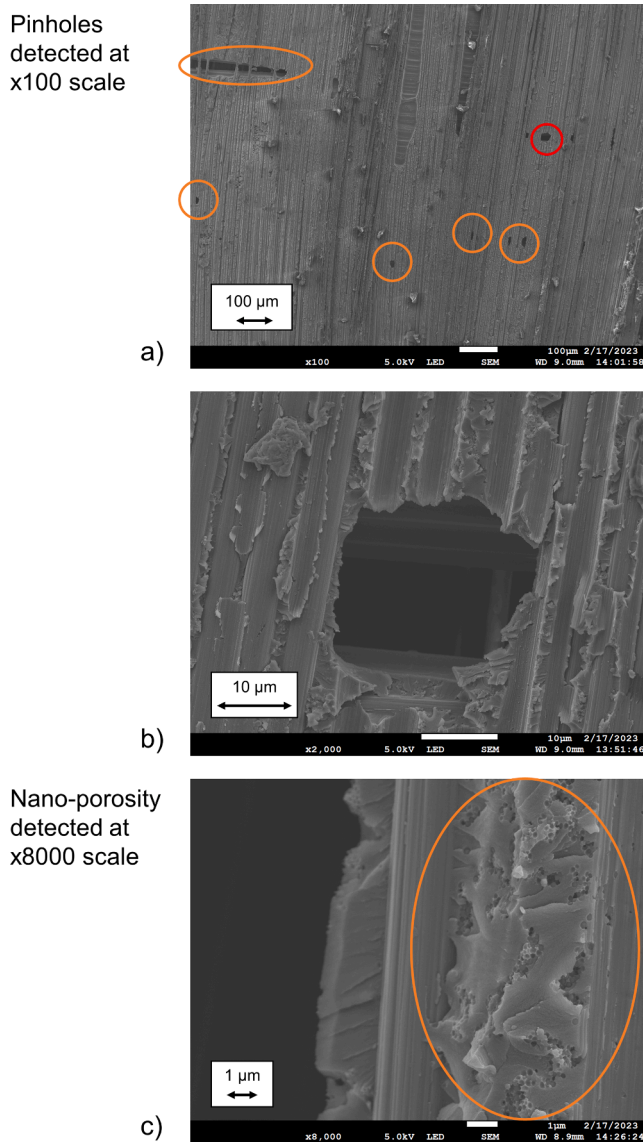| Batch	Permeation at 25 °C (Barrer)	Permeation activation energy (kJ mol^{-1})	Diffusivity at 25 °C (m^2 s^{-1})	Diffusion activation energy (kJ mol^{-1})
A1	0.091	31.9	5.24×10^{-12}	26.6
A2	0.103	26.7	7.98×10^{-11}	24.6
A3	Testing not completed			
B1	0.806	23.7	3.86×10^{-11}	27.2
B2$_{virgin}$	0.581	51.9	1.61×10^{-11}	17.3
B2$_{1\%}$	0.637	34.6	1.64×10^{-11}	18.2
B2$_{1.4\%}$	0.414	23.8	1.03×10^{-11}	21.4

Fig. 9. SEM imaging for material A3 across different scales. The magnifications considered were a) x100, b) x2000, c) x8000. (For interpretation of the references to colour in this figure legend, the reader is referred to the web version of this article.)
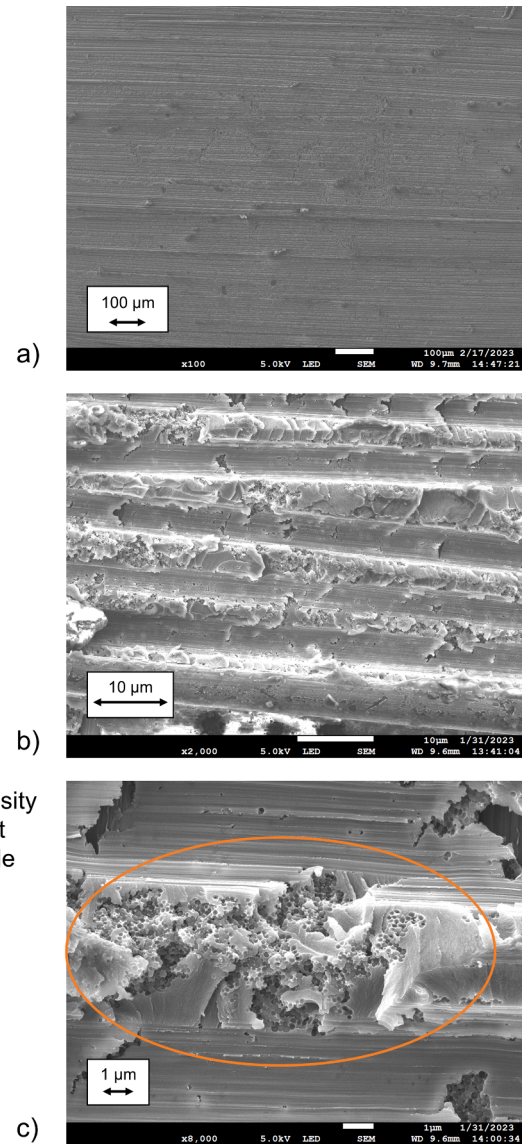
Fig. 10. SEM imaging for material A1 across different scales. The magnifications considered were a) x100, b) x2000, c) x8000. (For interpretation of the references to colour in this figure legend, the reader is referred to the web version of this article.)

morphology down to sub-nano scale (H_2 kinetic diameter is 0.289 nm).

5. Discussion

The values of permeability and diffusivity determined during the experimental campaign and reported in section 4 were used for a case study on the leak rate of a conceptual tank design. The design of the tank was based on work carried out in the LH2-tanks project [32]. The considered tank consists of a cylindrical part with a diameter of 300 mm and a height of 500 mm and two end caps with a spherical shape. A wall thickness of 2 mm was used in this case study which was based on a preliminary FE analysis.

The tank manufactured for the LH2-tanks project was made of thin-ply CFRP in the cylinder, titanium in the end caps while adhesive joints were connecting the two different parts. For simplicity, in this case study, the same CFRP material (material B2) was considered for both the cylinder and the end caps, and no adhesive joints were considered. Based on the dimensions, the total volume of the tank was calculated as 0.049 m^3 while the surface area of the inner walls of the tank was

calculated as 0.75 m^2.

As discussed in the previous sections, the permeability and diffusivity of the CFRP material follow an Arrhenius relationship and therefore their values can be extrapolated to temperatures of interest. More specifically, a range of temperatures were considered between 20 K (temperature of hydrogen liquefaction) and 293 K (room temperature). The case of the highest mechanical preloading (1.4% strain) was the one considered as the most conservative.

The leak rate was calculated as a flux governed by the pressure difference between the two sides of the laminate (pressure driving force), as shown in equation (7). In equations (7), J is the leak rate (molar flux), P is the permeability, Δp is the pressure difference and t is the thickness. The units of the leak rate are expressed as volume at Standard Temperature and Pressure (STP) over area per unit time. The pressure difference examined was 2, 50 and 700 bar which can be considered standard values for non-pressurised, intermediate, and pressurised vessels.
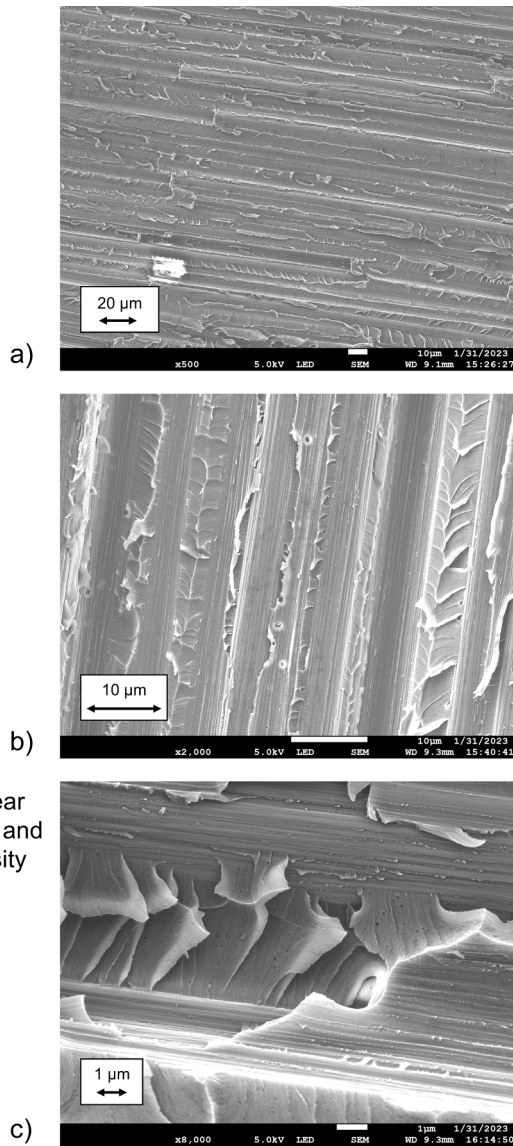
Fig. 11. SEM imaging for material B1 across different scales. The magnifications considered were a) x500, b) x2000, c) x8000.

Material clear of pinholes and nano-porosity

$$J = P\frac{\Delta p}{t} \tag{7}$$

Standardised allowable leak rates are currently lacking for composite hydrogen storage and are expected to be application dependent. For instance, Robinson [33] attempted to establish allowable leak rates for composite cryogenic tanks for launch vehicles. This was achieved by establishing allowable gas loss (0.25%) due to permeation and was based on Boeing's launch vehicle propulsion technology. Different allowable leak rates (scc m^{-2} s^{-1}) were established based on the operation and the lowest one (0.00574 scc m^{-2} s^{-1}) was chosen to be compared to the data from this study as the most conservative. However, it is worth noting, the allowable leak rate established in [33] is not considered very conservative for conventional transportation vehicles as it was designed for launch vehicles which only need to be fuelled once and do not require dormancy times such as aircraft or land vehicles.

Another allowable leak rate which is typically employed by the industry is based on a draft of an ISO standard [34] related to hydrogen tanks for land vehicles. This allowable leak rate correlates the leaking hydrogen to the total volume of the tank per unit time (1% loss of total volume per day). The second allowable leak rate is much more

conservative and about 3 orders of magnitude lower than the first one. Fig. 12 plots the values obtained in this study and compares them with the two allowable leak rates after converting them to consistent units.

Fig. 12 shows that for the low pressure (2 bar), the leak rates obtained in this study do not exceed the two limits even for higher temperatures (>400 K). However, for the case of intermediate (50 bar) and pressurised tanks (700 bar), the most conservative limit is exceeded at about 290 K and 230 K respectively, while the higher limit is not exceeded for the temperatures of interest. This shows that a combination of high pressures and lower temperatures might be needed to optimise the energy density of hydrogen and ensure leak free tanks. In addition, this case study is limited to a specific wall thickness value (2 mm). It is expected that the wall thickness will be significantly higher for pressurised tanks leading to lower values of leak rates as per equation (7).

It is worth noting that Fig. 12 is plotted by extrapolating the permeability values in low temperatures far from the experimental measurements. This extrapolation might introduce errors due to the experimental scatter. However, as shown in Fig. 12, the critical temperatures are close to the experimental measurements since permeability (and therefore the leak rate) minimise when the temperature drops below 200 K.

It can be concluded that thin-ply CFRP composites can be a suitable option for hydrogen storage tanks considering that they can provide adequate strength and stiffness, low permeability and diffusion rates at low density and therefore lead to significant weight reductions in the tank design. Moreover, the low values of permeability and diffusivity reported, despite the mechanical loading, show that liner-less options can be explored in the future. This is a direct result of using thin plies which can supress the generation of cracks at high strain levels (1.4%) and thus could prevent fast diffusion paths from forming.

It is worth noting however, that the performance of the material is controlled by the quality of the manufacturing. It was shown that defects (such as pinholes and dry spots) in μm scale could allow faster hydrogen permeation through the laminate thickness. It is therefore important to design and manufacture the tank in a way that the overall performance is not governed by defects on the ply level and that an adequate number of plies is used to ensure both low permeation rates and structural integrity.

One important aspect relating to the design of composite hydrogen storage tanks is the well-defined stress state which is experienced by the composites. The optimum fibre winding angle for the tanks has been determined as [+55/-55] which leads to equal circumferential and radial stresses. The cross-ply laminates studied here differ compared to the optimum angle laminates, but no significant performance changes
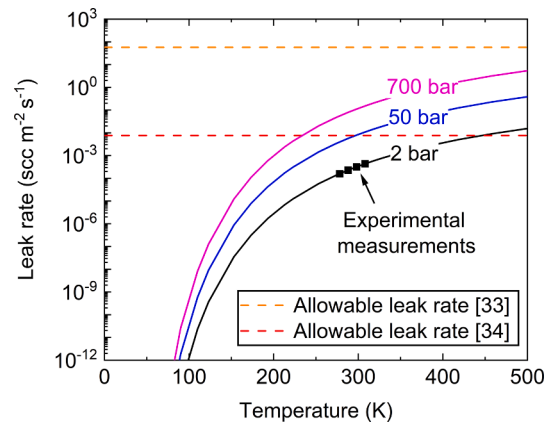

Fig. 12. Leak rates for non-pressurised, intermediate, and pressurised tanks over a range of temperatures and allowable leak rates. The higher allowable leak rate relates to launch vehicles while the lower allowable leak rate relates to land vehicles. (For interpretation of the references to colour in this figure legend, the reader is referred to the web version of this article.)

are expected. In the unloaded state, the hydrogen transport takes place through the laminate thickness and thus the permeability measurements would not get affected by the local ply orientation. The response after mechanical loading is also expected to remain unaffected as the optimum winding angle is expected to lead to lower developed strains compared to the cross-ply laminates studied here and thus no transverse cracking is expected to occur for the strain levels examined in this work.

Finally, it needs to be highlighted that hydrogen storage tanks experience a complex stress state and thermal cycles which lead to significant thermal residual stresses. Therefore, the design of such tanks would need to consider the complex stress states described above which would require more testing data. However, even these complex stress states are not expected to generate tensile strains exceeding 1.4% and thus our study was considered adequate in characterising the hydrogen transport phenomena after the application of mechanical loading.

6. Conclusions

The present study focuses on understanding the hydrogen permeability mechanism through thin-ply composites and the main conclusions follow:

- Despite the increased associated costs, thin-ply composites provide an alternative material that can be used for hydrogen storage tanks as they provide the necessary strength and stiffness with excellent sealing properties in the unloaded state.
- The hydrogen diffusivity of the thin-ply composites was shown to be higher (2–3 orders of magnitude) compared to more conventional materials such as metals. The values measured were consistent with similar studies for CFRP materials found in the literature.
- It was shown experimentally that a pre-loading up to 1.4% of tensile strain did not generate micro-cracks or damage that would accelerate the diffusion mechanism. This is considered very safe as the material in the tank is expected to experience strains at least 3 times lower.
- Manufacturing defects such as dry spots and pinholes, even at a μm scale can create fast diffusion paths and consequently make the material non-suitable for hydrogen storage. SEM analysis demonstrated such defects and correlated them to unsuccessful permeation measurements. Therefore, ensuring high quality manufacturing is critical for such applications. The presence of defects highlights the need for the development of sensors with the ability to detect hydrogen leakage.
- A study on a conceptual tank design revealed very low values of the leak rate at different values of pressure at the cryo range. At higher temperatures, the leak rates increased significantly but were still below the allowable limits fort most combinations of temperature and pressure. The parametric study also revealed that combinations of intermediate pressures and temperatures might need to be used as well as adjusting the thickness of the tank. These observations highlight the suitability of thin-ply composites for hydrogen storage applications.

CRediT authorship contribution statement

Ioannis Katsivalis: Conceptualization, Methodology, Investigation, Formal analysis, Data curation, Writing – original draft. **Virginia Signorini:** Methodology, Investigation, Formal analysis, Writing – review & editing. **Fredrik Ohlsson:** Resources, Writing – review & editing. **Christoph Langhammer:** Funding acquisition, Writing – review & editing. **Matteo Minelli:** Conceptualization, Methodology, Investigation, Formal analysis, Writing – review & editing. **Leif E. Asp:** Conceptualization, Methodology, Formal analysis, Supervision, Funding acquisition, Writing – review & editing.

Declaration of Competing Interest

The authors declare that they have no known competing financial interests or personal relationships that could have appeared to influence the work reported in this paper.

Data availability

Data will be made available on request.

References

[1] International Energy Agency. Transport. Paris: IEA; 2022.
[2] United Nations, Adoption of the Paris Agreement, Framework Convention on Climate Change/21st Conference of the Parties, Paris, United Nations; 2015.
[3] Andersson J, Grönkvist S. Large-scale storage of hydrogen. Int J Hydrogen Energy 2019;44:11901–19.
[4] Li H, Cao X, Liu Y, Shao Y, Nan Z, Teng L, et al. Safety of hydrogen storage and transportation: An overview on mechanisms, techniques, and challenges. Energy Rep 2022;8:6258–69.
[5] Martínez-Pañeda E, Golahmar A, Niordson CF. A phase field formulation for hydrogen assisted cracking. Comput Methods Appl Mech Eng 2018;342:742–61.
[6] Langmi HW, Engelbrecht N, Modisha PM, Bessarabov D. Chapter 13 - Hydrogen storage. In: Smolinka T, Garche J, editors. Electrochemical Power Sources: Fundamentals, Systems, and Applications. Elsevier; 2022. p. 455–86.
[7] Su Y, Lv H, Zhou W, Zhang C. Review of the Hydrogen Permeability of the Liner Material of Type IV On-Board Hydrogen Storage Tank. World Electric Vehicle J 2021.
[8] Disdier S, Rey JM, Pailler P, Bunsell AR. Helium permeation in composite materials for cryogenic application. Cryogenics 1998;38:135–42.
[9] Kumazawa H, Hayashi H, Susuki I, Utsunomiya T. Damage and permeability evolution in CFRP cross-ply laminates. Compos Struct 2006;76:73–81.
[10] Yokozeki T, Ogasawara T, Aoki T, Ishikawa T. Experimental evaluation of gas permeability through damaged composite laminates for cryogenic tank. Compos Sci Technol 2009;69:1334–40.
[11] Hamori H, Kumazawa H, Higuchi R, Yokozeki T. Numerical and experimental evaluation of the formation of leakage paths through CFRP cross-ply laminates with leak barrier layers. Compos Struct 2019;230:111530.
[12] Flanagan M, Grogan DM, Goggins J, Appel S, Doyle K, Leen SB, et al. Permeability of carbon fibre PEEK composites for cryogenic storage tanks of future space launchers. Compos A Appl Sci Manuf 2017;101:173–84.
[13] Saha S, Sullivan RW, Baker ML. Gas permeability mitigation of cryogenically cycled stitched composites using thin plies. Compos Struct 2023;304:116352.
[14] Grogan DM, Leen SB, Semprimoschnig COA, Ó Brádaigh CM. Damage characterisation of cryogenically cycled carbon fibre/PEEK laminates. Composites Part A: Appl Sci Manuf, 2014; 66: 237-50.
[15] Camanho PP, Dávila CG, Pinho ST, Iannucci L, Robinson P. Prediction of in situ strengths and matrix cracking in composites under transverse tension and in-plane shear. Compos A Appl Sci Manuf 2006;37:165–76.
[16] Galos J. Thin-ply composite laminates: a review. Compos Struct 2020;236:111920.
[17] Yokozeki T, Aoki Y, Ogasawara T. Experimental characterization of strength and damage resistance properties of thin-ply carbon fiber/toughened epoxy laminates. Compos Struct 2008;82:382–9.
[18] Hamori H, Kumazawa H, Higuchi R, Yokozeki T. Gas permeability of CFRP cross-ply laminates with thin-ply barrier layers under cryogenic and biaxial loading conditions. Compos Struct 2020;245:112326.
[19] Condé-Wolter J, Ruf MG, Liebsch A, Lebelt T, Koch I, Drechsler K, et al. Hydrogen permeability of thermoplastic composites and liner systems for future mobility applications. Compos A Appl Sci Manuf 2023;167:107446.
[20] Ebermann M, Bogenfeld R, Kreikemeier J, Glüge R. Analytical and numerical approach to determine effective diffusion coefficients for composite pressure vessels. Compos Struct 2022;291:115616.
[21] San Marchi C, Somerday BP. Technical Reference for Hydrogen Compatibility of Materials (SAND2012-7321), Sandia Report, Sandia National Laboratories, Livermore, CA; 2012.

[22] ASTM, D1434-82(2015)e1, Standard Test Method for Determining Gas Permeability Characteristics of Plastic Film and Sheeting, ASTM International, West Conshohocken, PA; 2016.

[23] Crank J. The mathematics of diffusion. Oxford University Press; 1979.

[24] Costello LM, Koros WJ. Temperature dependence of gas sorption and transport properties in polymers: measurement and applications. Ind Eng Chem Res 1992;31: 2708–14.

[25] Chen SS, Wu TI, Wu JK. Effects of deformation on hydrogen degradation in a duplex stainless steel. J Mater Sci 2004;39:67–71.

[26] Hutchings RB, Turnbull A, May AT. Measurement of hydrogen transport in a duplex stainless steel. Scr Metall Mater 1991;25:2657–62.

[27] Luu WC, Liu PW, Wu JK. Hydrogen transport and degradation of a commercial duplex stainless steel. Corros Sci 2002;44:1783–91.

[28] Young GA, Scully JR. The diffusion and trapping of hydrogen in high purity aluminum. Acta Mater 1998;46:6337–49.

[29] Saitoh H, Iijima Y, Tanaka H. Hydrogen diffusivity in aluminium measured by a glow discharge permeation method. Acta Metall Mater 1994;42:2493–8.

[30] Outlaw RA, Peterson DT, Schmidt FA. Diffusion of hydrogen in pure large grain aluminum. Scr Metall 1982;16:287–92.

[31] Katsivalis I, Persson M, Johansen M, Moreau F, Kullgren E, Norrby M, et al. Strength analysis and failure prediction of thin tow-based discontinuous composites. Compos Sci Technol 2023.

[32] Tanks for Liquid Hydrogen, 2023, RISE Research Institutes of Sweden, https://www.ri.se/en/what-we-do/projects/tanks-for-liquid-hydrogen, Accessed 01/05/2023.

[33] Robinson MJ. Determination of Allowable Hydrogen Permeation Rates for Launch Vehicle Propellant Tanks. J Spacecr Rocket 2008;45:82–9.

[34] ISO, DD ISO/TS 15869:2009 Gaseous hydrogen and hydrogen blends — Land vehicle fuel tanks, British Standards International, London; 2009.